HHS Public Access

Author manuscript

Life Sci. Author manuscript; available in PMC 2019 January 07.

Published in final edited form as:

Life Sci. 2018 June 15; 203: 39–47. doi:10.1016/j.lfs.2018.04.017.

Slit2-Robo2 signaling modulates the fibrogenic activity and migration of hepatic stellate cells

Zhiping Zeng[a], **Yujing Wu**[a], **Yirong Cao**[a], **Ziying Yuan**[a], **Yuanqing Zhang**[a], **David Y. Zhang**[b], **Daisuke Hasegawa**[b], **Scott L. Friedman**[b], and **Jinsheng Guo**[a,*]

[a]Division of Digestive Diseases, Zhongshan Hospital, Fu Dan University, Shanghai 200032, PR China

[b]Division of Liver Diseases, Icahn School of Medicine at Mount Sinai, New York 10029, NY, USA

Abstract

Background & aim: Slit/Robo signaling was originally identified as a repulsive guidance cue in regulating axon branching and neuronal migration. Hepatic stellate cells (HSCs) are the key fibrogenic cells in the liver, which are migratory when activated, and express neural crest markers. The aim of the present study was to investigate the functional significance of Slit/Robo signaling in liver fibrogenesis and in HSCs.

Key findings: By transcriptomic analysis it was found that axon guidance signaling pathways were significantly upregulated in both diethylnitrosamine (DEN) and thioacetamide (TAA)-induced experimental liver fibrosis. The up-regulation of the ligand Slit2 and membrane receptor Robo2 genes within this pathway was further validated in TAA-induced fibrotic livers. By immunofluorescence staining, Robo2 was localized in fibrotic septa of fibrotic liver and on the surface of HSCs. By Western blot analysis, recombinant Slit2 (rSlit2) was found to promote fibrogenic protein expression in JS1 cells, an immortalized mouse HSC line, while activating PI3K/Akt signaling pathway. This effect was abrogated by LY294002, a PI3K/Akt pathway inhibitor. In addition, rSlit2 stimulation markedly inhibited JS1 cells migration in transwell migration assays, which was abrogated by small interfering RNA (siRNA) knockdown of Robo2 in the cells.

Significance: The present study provides evidence that Slit2/Robo2 signaling mediates the pathogenesis of hepatic fibrogenesis and regulates HSCs biology, thus providing potential markers for HSCs, and therapeutic and diagnostic target toward liver fibrosis.

Keywords

Liver fibrosis; Slit2; Robo2; Hepatic stellate cells; Signaling pathway; Cell migration

*Corresponding author at: Division of Digestive Diseases, Zhong Shan Hospital, Fu Dan University, 180 Feng Lin Road, Shanghai 200032, PR China., guo.jinsheng@zs-hospital.sh.cn (J. Guo).

Conflict of interest

The authors declare no conflict of interest.

Supplementary data to this article can be found online at https://doi.org/10.1016/j.lfs.2018.04.017.

1. Introduction

Hepatic fibrosis is a characteristic consequence of multiple chronic liver injuries, including metabolic disorders, toxins, viral hepatitis, steatohepatitis and autoimmune diseases [1–3]. During liver fibrosis, chronic inflammation, tissue repair and excessive accumulation of extracellular matrix (ECM), especially collagen, contribute to liver dysfunction and ultimately to irreversible cirrhosis [3–7]. Although several other cell types may also participate in the development of liver fibrosis, hepatic stellate cells (HSCs) have been recognized as the primary cells responsible for ECM deposition [3,8,9]. The activation of HSCs is the central event in fibrogenesis. Activated HSCs adopt a myofibroblastlike phenotype and release profibrogenic and promitogenic cytokines, produce collagen and other ECM components, acquire chemotactic abilities which confer upon them the potential to migrate and accumulate. HSCs express neural crest markers such as glial fibrillary acidic protein (GFAP) and genes that belong to axon guidance pathways ordinarily found in neuronal cells, implicating HSCs might have a neural crest origin [10,11].

Slit/Robo signaling pathway belongs to axon guidance signaling transduction pathways and was initially characterized as a repulsive cue to guide the direction of neuronal migration during nervous system development [12]. It is comprised of the Slit family (Slit1–3) and four known receptors (Robo1–4). The membrane protein Robo2 receptor was found to be inducible by the secreted glycoprotein Slit2 in mammals, which serve as a chemorepellent to affect cell migration [13]. Previous studies have also found that Slit2 inhibits leukocytes chemotaxis, as well as the migration of vascular smooth muscle cells and breast cancer cells [14–16]. Moreover, aberrant expression of the Slit/ Robo genes has been observed in several human cancers, including hepatocellular carcinoma [17]. However, the functional significance of Slit/Robo signaling in liver fibrogenesis and its impact on HSC biology remain unclear. In the present study, the changing profile of genes belonging to axon guidance signaling pathways during liver fibrogenesis was detected by transcriptomic analysis of the liver tissues. The altered expression of Slit2 and Robo2 molecules, as well as the immune-localization of Robo2 protein were further investigated in vivo in mice models of liver fibrosis and in vitro in an immortalized mouse HSC line, JS1. The impact of Slit2/ Robo2 activation on the fibrogenic and migration activities of HSCs was further investigated in vitro in JS1 cells with the introduction of recombinant Slit2 (rSlit2) and small interfering RNA (siRNA) of Robo2.

2. Materials and methods

2.1. Ethics statement

The study protocol was approved by the committee on the use of live animals for teaching and research of Zhong Shan Hospital (No. 2011–131), Fu Dan University, and performed in accordance with the National Institutes of Health (NIH) guide for the care and use of Laboratory animals.

2.2. Animal models of hepatic fibrosis

Male C57BL/6J mice about 4-week-old weighting between 15 and 20 g were obtained from the Animal Research Center of Fu Dan University. Two experimental models of hepatic fibrosis were employed by intraperitoneal injections of diethylnitrosamine (DEN, 10 mg/kg/week) or thioacetamide (TAA, 100 mg/kg, three times per week) in mice for 14 weeks. Mice in the control groups received the same volume of normal saline intraperitoneally. Liver samples were collected from three mice in the control and 5 mice in the treatment groups at different time points post DEN or TAA treatment and storage at −80 °C for RNA and protein analysis. A part of each liver samples were fixed in 10% buffered formalin for histologically assessment of the progression of liver fibrosis. Blood samples were collected from portal veins of the mice and the serum were stored in −80 °C for subsequent ELISA analysis.

2.3. Bioinformatics analysis

Total RNA was extracted with Trizol reagent (Invitrogen, Carlsbad, CA, USA) and purified using RNeasy Mini Kit (Qiagen, Valencia, CA). Liver transcriptomes were obtained by high throughput RNA sequencing. Time-series and tendency analysis were performed to obtain the unanimous changed expression genes during liver fibrosis, followed by gene ontology and pathway analyses. Biological pathways with significant enrichment of the differentially expressed genes were identified according to latest Kyoto Encyclopedia of Genes and Genomes (KEGG) database. Enrichment provides a measure of the significance of the function, and the threshold of significance was defined as P value < 0.01 and the false discovery rate (FDR) < 0.05.

2.4. Histological and immunofluorescence staining

Formalin-fixed liver tissues were embedded in paraffin. Morphological examination was performed with hematoxylin and eosin (H&E) staining for histological assessment of the progression of liver fibrosis. Masson's trichrome and reticulin staining were used to demonstrate fibrotic changes and collagen deposition.

Frozen liver tissue sections were prepared from mice treated with TAA for 6 weeks. The sections were fixed with ice-cold acetone for 5 min, permeabilised with 0.1% Triton X-100 in PBS for 15 min, blocked with normal goat serum diluted 1:20 for 30 min. Staining was performed with primary mouse McAb to Robo2 or rabbit PcAb to Desmin (Abcam, Cambridge, MA, USA) diluted 1:100 and 1:500 fold respectively at 4 °C overnight. Primary antibody detection was performed with Alexa Fluor 488-conjugated goat anti-rabbit or Alexa Fluro 647-conjugated goat anti-mouse IgG. The slide was mounted by Prolong Gold antifade reagent (Invitrogen) and examined using a Zeiss Axiophot microscope (Carl Zeiss, Oberkochen, Germany).

2.5. Enzyme-linked immunosorbent assay (ELISA)

Serum levels of Slit2 were analyzed using commercially available ELISA kits (Cusabio Biotech Co., Wuhan, China) according to the manufacturer's instructions. The optical density was measured at 450 nm using a microplate reader. All samples were assayed triplicate repeats and values were expressed as mean ± SD.

2.6. Cell culture

The immortalized wild type mouse HSC line JS1 was generated and described in our previous studies [18,19]. The cells were maintained in Dulbecco's Modified Eagle's Medium (DMEM) (Gibco, Invitrogen) supplemented with 10% fetal bovine serum (FBS) (Gibco, Invitrogen) and antibiotics at 37 °C in a 5% CO2 humidified atmosphere. In certain experiments, JS1 cells were treated with recombinant mouse Slit2 protein (R&D Biosystems, Minneapolis, MN, USA) at final concentrations of 100 or 500 ng/mL, or PBS vehicle for 24 h. To inhibit Akt, cells were exposed to the Phosphatidylinositol 3-kinase (PI3K) inhibitor, LY294002 (25 μM, Cell Signaling Technology, Danvers, MA, USA) for 1 h. The selection of Slit2 and LY294002 concentration was referred to literatures [20,21].

2.7. siRNA transfection assays

JS1 cells were transfected with Robo2 siRNA and the negative control siRNA using the TurboFect Transfection Reagent (Thermo Fisher Scientific, Waltham, MA, USA) according to the manufacturer's instructions. The sequences of Robo2-specific siRNA were 5′-GACCAA UAAACCAAACACUTT-3′ (sense) and 5′-AGUGUUUGGUUUAUUGGU CTT-3′ (antisense). The negative control sequences were 5′-UUCUCCG AACGUGUCACGUTT-3′ (sense) and 5′-ACGUGACACGUUCGGAGA ATT-3′ (antisense). The final concentration of siRNA and negative control used for transfection was 100 nM. Knockdown efficiency was verified by Real-Time quantitative PCR (RT-qPCR) and Western blot.

2.8. Real-time quantitative PCR

Total RNA was isolated from liver tissues and JS1 cells using TRIzol reagent (Invitrogen, Carlsbad, CA) according to the manufacturer's instructions. The cDNA was performed using PrimeScript RT Master Mix (Takara, Bio, Shiga, Japan) on the GeneAmp® PCR system 9700 (Applied Biosystems, CA, USA) and the RT-qPCR analyses were conducted by using SYBR Green PCR master mix (Takara, Tokyo, Japan) in the 7500 real-time PCR system (Applied Biosystems, Thermo Fisher Scientific, Waltham, MA, USA). GAPDH (B661304, Sangon Biotech, Shanghai, China) was used as an internal control. Robo2 primers were obtained from Yijin (MQP041372, Guangzhou, China). Other primer sequences (Sangon Biotech, Shanghai, China) for primers are listed as follows: α-SMA forward, 5′-GGCACCACTGAACCCTAAGG-3′ and reverse, 5′-ACAATAC CAGTTGTACGTCCAGA-3′; Col1-α1 forward, 5′-TGACTGGAAGAGCGGAG AGT-3′ and reverse, 5′-GACGGCTGAGTA GGGAACAC-3′; and Slit2 forward, 5′-GGCAGACACTGTCCCTATCG-3′ and reverse, 5′-GTGTTGCGGGGGATATTCCT-3′. The mRNA expression levels of Robo2, α-SMA, Col1-α1, and Slit2 were normalized to that of GAPDH.

2.9. Western blot analysis

Liver tissues and JS1 cells were prepared on ice with RIPA lysis buffer (Beyotime, Shanghai, China) containing 1mM phenylmethylsulfonyl fluoride (Beyotime) for total protein and PhosStop phosphatase inhibitors (Roche, Indianapolis, IN., USA) for phosphorylated protein. Equal amounts of protein were separated by 8% SDS-PAGE and

transferred onto polyvinylidene difluoride (PVDF) membranes (Millipore Corp., Billerica, MA, USA). Membranes were blocked with 5% non-fat milk in TBST buffer for 1 h at room temperature and then incubated overnight at 4 °C with the following primary antibodies: rabbit monoclonal anti-Slit2 (1:1000, ab134166), rabbit polyclonal anti-Robo2 (1:500, ab75014), rabbit polyclonal anti-Col-1 (1:5000, ab34710), mouse monoclonal anti-α-SMA (1:250; ab7817), and rabbit polyclonal anti-CTGF (1:1000, ab6992) (Abcam, Cambridge, MA, USA); rabbit polyclonal anti-TGF-β1 (1:250, proteintech, 18978–1-AP); Akt (4691), P-Akt (13038), PI3K (4249), P-PI3K (4228) (Cell Signaling Technology, Danvers, MA, USA). Membranes were washed and incubated with peroxidase-conjugated secondary antibodies (Yeasen, Shanghai, China) for 1 h at room temperature. The signals were visualized by enhanced chemiluminescence (ECL) method using chemiscope 5600 (CLINX, Shanghai, China). GAPDH (5174, Cell Signaling Technology, Danvers, MA, USA) was used as a loading control. The protein signals were semi-quantitative analyzed by densitometric scanning.

2.10. Cell migration assay

JS1 cells with or without siRNA transfection were resuspended in serum-free DMEM (4×10^4 cells/200 μL/well) and seeded in the upper chamber of the 8-μm-pore transwell filters (Costar, Lowell, MA, USA). The lower chambers were supplemented with 500 μL 10% FBS/DMEM containing different concentrations of recombinant mouse Slit2 protein (0, 100, 500 ng/mL) (R&D Biosystems, Minneapolis, MN, USA). Cells treated with vehicle were used as a control. After incubation for 24 h at 37 °C, cells were then fixed with 4% paraformaldehyde and stained with Giemsa. The number of cells that migrated to the bottom side of the insert was counted in 10 randomly selected fields under microscope with 20× magnification.

2.11. Statistical analyses

All data were represented as the mean ± standard deviation (SD). Statistical analysis was performed using SPSS 20.0 (SPSS Inc., Chicago, IL, USA). Student's *t*-test (two-tailed) and one-way analysis of variance (ANOVA) respectively were used to compare two groups and multiple-group analysis. A value of $P < 0.05$ was considered statistically significant.

3. Results

3.1. Activation of axon guidance signaling with the progression of hepatic fibrogenesis

To identify the novel signaling pathways and key molecules that are involved in liver fibrogenesis, liver samples collected from mice at different time points following DEN or TAA treatment were analyzed by RNA sequencing and transcriptomic analysis. Pathway analysis revealed that axon guidance signaling pathways were significantly upregulated in fibrotic livers of both DEN and TAA models (Tables 1 and 2). In the transcriptomes of fibrotic livers, forty-eight differentially expressed genes in DEN model and 23 differentially expressed genes in TAA model were enriched in axon guidance signaling pathways. Both included genes encoded the ligands (e.g., Slit2, Sema5 and 4D), membrane receptors (e.g., Robo1, Robo2, CXCR4), downstream kinases (e.g., PAK and ROCK) (Fig. 1). The results

indicated that axon guidance signaling pathways activated and contributed to liver fibrogenesis.

3.2. Induction of hepatic fibrosis in TAA and DEN treated mice

H&E staining, Masson's trichrome and reticulin staining were performed to assess the stage of liver fibrosis (Fig. 2A). Compared to normal mouse liver, the liver tissues from mice treated with TAA demonstrated marked fatty degeneration, cell necrosis, inflammatory cell infiltration and fibrous septa forming. Control livers showed normal hepatic architecture. At weeks 3, 6 and 9, collagen deposition started to occur in the centrilobular regions among degenerating hepatocytes, forming thin fibrous septa. At week 14, fibrous bridges became thicker with excessive deposition of collagen fibers, forming large fibrous septa surrounding the lobules (Fig. 2A). The relative mRNA (Fig. 2B, C) and protein (Fig. 2D) expression of the fibrogenic markers of activated HSCs, such as α-SMA and collagen type I (Col-1), were significantly increased in progressive stages of liver fibrosis when compared to control mice livers, consistent with the morphological changes.

H&E staining for the liver histology of DEN-treated mice showed similar fibrogenic changes (Supplementary Fig. 1). Extensive inflammatory cell infiltration along with hepatocyte dysplasia was observed in the livers of mice with DEN treatment for 14 weeks. No significant tumor mass was observed during the experimental period of time.

As DEN is a model of liver carcinogenesis which is usually used in combination with carbon tetrachloride to study the sequence liver fibrosis with subsequent development of a hepatocellular carcinoma, TAA model is well accepted and documented to study liver fibrosis, we next focused on TAA model to validate the participation of axon guidance signaling pathways in liver fibrosis progression.

3.3. Localization of Robo2 in hepatic tissues and an activated HSC line

In the liver samples with TAA-induced fibrosis, the expression and distribution of Robo2 correlated well with the fibrotic septa in fibrotic livers, and were on the surface of cells shown double-positive staining with desmin in the cytoplasm (Fig. 3A). In vitro immunofluorescence staining of Robo2 of JS1 demonstrated that the protein was localized on the cell surface (Fig. 3B). These results indicated that Robo2 was a novel activated HSC' surface marker and contributed to liver fibrogenesis by this cell type.

3.4. Expression of Slit2 and Robo2 are upregulated in hepatic fibrotic tissues

The mRNA and protein expression of Slit2 and its receptor Robo2 in normal liver and hepatic fibrosis tissues were examined by qRT-PCR and Western blotting, respectively. Both mRNA (Fig. 4A, B) and protein (Fig. 4C) expression levels of Slit2 and Robo2 were markedly increased with the progression of liver fibrosis induced by TAA when compared to control liver. The serum level of Slit2 was also significantly higher in mice with liver fibrosis than in the control group (Fig. 4D). These results confirmed that the expression of key signaling molecules of axon guidance signaling, i.e., the ligand Slit2 and the membrane receptor Robo2, were upregulated in fibrotic livers, suggesting a role of this signaling in liver fibrogenesis.

3.5. Slit2 induces fibrogenic factor production via PI3K/Akt pathway

Western blot for PI3K/Akt pathway members demonstrated that rSlit2 (100 ng/mL) induced PI3K and Akt phosphorylation (Fig. 5A), and increased the levels of fibrogenic factors in JS1 cells, including Col1, TGF-β1 and CTGF. These effects were abrogated by pre-treating the cells with a PI3K inhibitor LY294002 (25 μM) for 1 h prior to the stimulation with rSlit2 (Fig. 5B). The results indicated that PI3K/Akt signaling pathway contribute to the Slit2-induced up-regulation of fibrogenic factors production in HSCs.

3.6. rSlit2 inhibits JS1 cell migration via binding to Robo2

Transwell migration assay was performed to examine the effect of Slit2 on HSC migration. Compared to control JS1 cells, the number of migrated cells was significantly decreased in rSlit2-treated JS1 cells in a dose dependent manner (Fig. 6C). The inhibitory effect of Slit2 on HSC migration was abrogated by Robo2 knock-down in JS1 cells using specific siRNA, along with significantly down-regulated mRNA expression of Robo2 by qRT-PCR analysis (Fig. 6B) and Robo2 protein by Western blot (Fig. 6A). These data demonstrated that the effect of Slit2 on HSCs migration was mediated by the Robo2 receptor.

4. Discussion

In this study, axon guidance signaling pathways were found to be significantly upregulated during the development of experimental liver fibrosis. The membrane receptor Robo2 of these signaling pathways was localized in fibrotic septa of fibrotic liver and on the surface of HSCs. The interaction of Robo2 and its ligand Slit2 promoted the fibrogenic activity of HSCs whereas it inhibited the cell migration.

Hepatic fibrosis is the wound healing and scarring response of liver in response to a variety of chronic insults [2]. Known fibrogenesis related receptors and signaling pathways that have been recognized previously including TGF-β-Smad, Renin-angiotensin-aldosterone, Integrin, and Toll-like receptors contribute to HSC activation and ECM accumulation in injured liver. HSCs is the major fibrogenic cell type and key cellular element involved in hepatic fibrogenesis [22], whenever the cells undergo phenotypic transformation from quiescent lipidstoring status into myofibroblasts with fibrogenic properties, specifically, producing ECM components and releasing fibrogenic mediators, such as TGF-β, PDGF, and CTGF [23,24]. In the present study, by using transcriptomic analysis, we found that axon guidance signaling pathways were also activated with the progression of hepatic fibrosis. The potential important function of these signaling in fibrogenesis was further indicated by the immune localization of the membrane receptor Robo2 in fibrotic septa of fibrotic liver and on the surface of HSCs. Moreover, our data revealed that rSlit2 markedly increased the expression of pro-fibrotic mediators (i.e., TGF-β1, CTGF) and major fibrotic ECM component (i.e., Col-1) in JS1 cells in vitro, indicating that Slit2/Robo2 signaling was involved in promoting liver fibrogenesis with a direct effect on HSCs. These findings are in line with a previous report by Chang et al., showing that liver injury and hepatic expression of collagen I and α-SMA were attenuated in $Robo1^{+/-}Robo2^{+/-}$ double heterozygotes mice in response to CCl4 exposure [25]. The present study emphasizes Robo2 location and function in HSCs, and further suggests an interaction or synergy effect between $Robo1^{+/-}$

and Robo2$^{+/-}$ to mediate Slit2 downstream signaling. This warrants further investigation in vivo using liver fibrosis model with specific inhibition of Slit2-Robo2 on HSCs.

The proliferation of activated HSCs plays a critical role in the progression of liver fibrosis, and the activation of HSCs is initiated partly via activating PI3K and ERK signaling. Inhibition of PI3K/Akt signaling in HSCs during liver fibrogenesis decreased TGF-β, CTGF, TIMP-1 expression and the deposition of type I collagen [26,27]. In this study, rSlit2 administration significantly induced PI3K/Akt phosphorylated activation in HSCs, along with increased expression of TGF-β1, CTGF, and Col-1. These effects were shown abrogated by PI3K inhibitor LY294002, indicating that PI3K/Akt mediate the down-stream pro-fibrotic effect of Slit2 on HSCs.

Slit and Robo have primarily been described in Drosophila as key regulators of commissural axon guidance. Robo2, a key receptor mediating axon guidance signaling, is essential for Slit ligand-mediated intra-retinal axon pathfinding [28]. The distribution of Slit/Robo was also reported in other tissue cell types with diverse functions including leukocyte recruitment [29], endothelial cells angiogenesis [30], adipose tissue thermogenesis and metabolic function [31], and cell differentiation [32]. Slit-Robo signaling has previously been shown to participate in regulating the migration of cancer cells [33,34], human umbilical vein endothelial cells (HUVEC) [35], and rat airway smooth muscle cells [20]. As a diffusible molecule, the concentration gradient of Slit was found to guide the direction of neuronal migration in the olfactory system [36]. The center-to-periphery gradient in solid tumors might contribute to the exaggerated angiogenesis in the tumor center [30]. In the present study, we demonstrated that rSlit2 inhibited HSC migration in a dose dependent manner. Slit2 interacting with the transmembrane protein Robo2 mediated the inhibitory activity of HSCs migration, as evidenced by Robo2 knocking-down in JS1 cells with specific siRNA abrogated the inhibitory effect of Slit2 on HSC migration. Thus, we hypothesize that Slit2 may also be expressed and distributed along a gradient in injured liver within the fibrogenic regions, so that it directs the HSCs migration. In addition, Slit2-Robo signaling is increasingly being recognized as an important regulator of vascular physiology in health and in disease [37–40]. As angiogenesis itself is a major modulator of liver fibrogenesis [41], the impact of Slit2-Robo2 inhibition on vascular remodeling of liver fibrosis warrants further investigation.

5. Conclusion

In conclusion, our study demonstrates that Slit2-Robo2 signaling reduces HSC migration but promotes production of pro-fibrogenic mediators, and the PI3K/Akt pathway is at least partly involved. These results indicate that Slit2-Robo2 signaling distinctively regulates biological signaling in HSCs, and might provide a potential therapeutic and diagnostic target toward hepatic fibrosis.

Acknowledgments

This work was supported by the National Fund of Nature Science of P.R. China (No., 91129705, 81070340), and RO1DK56621 NIH grant.

References

[1]. Bataller R, Brenner DA, Liver fibrosis J Clin. Invest 115 (2005) 209–218.

[2]. Fagone P, Mangano K, Pesce A, Portale TR, Puleo S, Nicoletti F, Emerging therapeutic targets for the treatment of hepatic fibrosis, Drug Discov. Today 21 (2016) 369–375. [PubMed: 26523773]

[3]. Friedman SL, Mechanisms of hepatic fibrogenesis, Gastroenterology 134 (2008) 1655–1669. [PubMed: 18471545]

[4]. Trautwein C, Friedman SL, Schuppan D, Pinzani M, Hepatic fibrosis: concept to treatment, J. Hepatol 62 (1 Suppl) (2015) S15–S24. [PubMed: 25920084]

[5]. Higashi T, Friedman SL, Hoshida Y, Hepatic stellate cells as key target in liver fibrosis, Adv. Drug Deliv. Rev (2017), 10.1016/j.addr.2017.05.007 (pii: S0169–409X(17)30063–7).

[6]. Rockey DC, Translating an understanding of the pathogenesis of hepatic fibrosis to novel therapies, Clin. Gastroenterol. Hepatol 11 (2013) 224–231. [PubMed: 23305825]

[7]. Bataller R, Brenner DA, Hepatic stellate cells as a target for the treatment of liver fibrosis, Semin. Liver Dis 21 (2001) 437–451. [PubMed: 11586471]

[8]. Elpek GÖ, Cellular and molecular mechanisms in the pathogenesis of liver fibrosis: an update, World J. Gastroenterol 20 (2014) 7260–7276. [PubMed: 24966597]

[9]. Lee YA, Wallace MC, Friedman SL, Pathobiology of liver fibrosis: a translational success story, Gut 64 (2015) 830–841. [PubMed: 25681399]

[10]. Ouyang Y, Guo J, Lin C, Lin J, Cao Y, Zhang Y, Wu Y, Chen S, Wang J, Chen L, Friedman SL, Transcriptomic analysis of the effects of Toll-like receptor 4 and its ligands on the gene expression network of hepatic stellate cells, Fibrogenesis Tissue Repair 9 (2016) 2, 10.1186/s13069-016-0039-z. [PubMed: 26900402]

[11]. Friedman SL, Hepatic stellate cells: protean, multifunctional, and enigmatic cells of the liver, Physiol. Rev 88 (2008) 125–172. [PubMed: 18195085]

[12]. Guan KL, Rao Y, Signalling mechanisms mediating neuronal responses to guidance cues, Nat. Rev. Neurosci 4 (2003) 941–956. [PubMed: 14682358]

[13]. Ji J, Li Q, Xie Y, Zhang X, Cui S, Shi S, Chen X, Overexpression of Robo2 causes defects in the recruitment of metanephric mesenchymal cells and ureteric bud branching morphogenesis, Biochem. Biophys. Res. Commun 421 (2012) 494–500. [PubMed: 22521888]

[14]. Wu JY, Feng L, Park HT, Havlioglu N, Wen L, Tang H, Bacon KB, Jiang Z, Zhang X, Rao Y, The neuronal repellent Slit inhibits leukocyte chemotaxis induced by chemotactic factors, Nature 410 (2001) 948–952. [PubMed: 11309622]

[15]. Liu D, Hou J, Hu X, Wang X, Xiao Y, Mou Y, De Leon H, Neuronal chemorepellent Slit2 inhibits vascular smooth muscle cell migration by suppressing small GTPase Rac1 activation, Circ. Res 98 (2006) 480–489. [PubMed: 16439689]

[16]. Prasad A, Paruchuri V, Preet A, Latif F, Ganju RK, Slit-2 induces a tumor-suppressive effect by regulating beta-catenin in breast cancer cells, J. Biol. Chem 283 (2008) 26624–26633. [PubMed: 18611862]

[17]. Avci ME, Konu O, Yagci T, Quantification of SLIT-ROBO transcripts in hepatocellular carcinoma reveals two groups of genes with coordinate expression, BMC Cancer 8 (2008) 392. [PubMed: 19114000]

[18]. Guo J, Loke J, Zheng F, Hong F, Yea S, Fukata M, Tarocchi M, Abar OT, Huang H, Sninsky JJ, Friedman SL, Functional linkage of cirrhosis-predictive single nucleotide polymorphisms of Toll-like receptor 4 to hepatic stellate cell responses, Hepatology 49 (2009) 960–968. [PubMed: 19085953]

[19]. Zhang Z, Lin C, Peng L, Ouyang Y, Cao Y, Wang J, Friedman SL, Guo JS, High mobility group box 1 activates toll like receptor 4 signaling in hepatic stellate cells, Life Sci. 91 (2012) 207–212. [PubMed: 22841886]

[20]. Ning Y, Sun Q, Dong Y, Xu W, Zhang W, Huang H, Li Q, Slit2-N inhibits PDGF-induced migration in rat airway smooth muscle cells: WASP and Arp2/3 involved, Toxicology 283 (2011) 32–40. [PubMed: 21315131]

[21]. Zhou Y, Tu C, Zhao Y, Liu H, Zhang S, Placental growth factor enhances angiogenesis in human intestinal microvascular endothelial cells via PI3K/Akt pathway: potential implications of inflammation bowel disease, Biochem. Biophys. Res. Commun 470 (2016) 967–974. [PubMed: 26775845]

[22]. Trautwein C, Friedman SL, Schuppan D, Pinzani M, Hepatic fibrosis: concept to treatment, J. Hepatol 62 (2015) S15–S24. [PubMed: 25920084]

[23]. Puche JE, Saiman Y, Friedman SL, Hepatic stellate cells and liver fibrosis, Compr. Physiol 3 (2013) 1473–1492. [PubMed: 24265236]

[24]. Inagaki Y, Okazaki I, Emerging insights into transforming growth factor beta Smad signal in hepatic fibrogenesis, Gut 56 (2007) 284–292. [PubMed: 17303605]

[25]. Chang J, Lan T, Li C, Ji X, Zheng L, Gou H, Ou Y, Wu T, Qi C, Zhang Q, Li J, Gu Q, Wen D, Cao L, Qiao L, Ding Y, Wang L, Activation of Slit2-Robo1 signaling promotes liver fibrosis, J. Hepatol 63 (2015) 1413–1420. [PubMed: 26264936]

[26]. Son G, Hines IN, Lindquist J, Schrum LW, Rippe RA, Inhibition of phosphatidylinositol 3-kinase signaling in hepatic stellate cells blocks the progression of hepatic fibrosis, Hepatology 50 (2009) 1512–1523. [PubMed: 19790269]

[27]. Muñoz-Félix JM, Fuentes-Calvo I, Cuesta C, Eleno N, Crespo P, López-Novoa JM, Martínez-Salgado C, Absence of K-Ras reduces proliferation and migration but increases extracellular matrix synthesis in fibroblasts, J. Cell. Physiol 231 (2016) 2224–2235. [PubMed: 26873620]

[28]. Thompson H, Andrews W, Parnavelas JG, Erskine L, Robo2 is required for slitmediated intraretinal axon guidance, Dev. Biol 335 (2009) 418–426. [PubMed: 19782674]

[29]. Chaturvedi S, Robinson LA, Slit2-Robo signaling in inflammation and kidney injury, Pediatr. Nephrol 30 (2015) 561–566. [PubMed: 24777535]

[30]. Wang B, Xiao Y, Ding BB, Zhang N, Yuan XB, Gui L, Qian KX, Duan S, Chen Z, Rao Y, Geng JG, Induction of tumor angiogenesis by Slit-Robo signaling and inhibition of cancer growth by blocking Robo activity, Cancer Cell 4 (2003) 19–29. [PubMed: 12892710]

[31]. Svensson KJ, Long JZ, Jedrychowski MP, Cohen P, Lo JC, Serag S, Kir S, Shinoda K, Tartaglia JA, Rao RR, Chédotal A, Kajimura S, Gygi SP, Spiegelman BM, A secreted Slit2 fragment regulates adipose tissue thermogenesis and metabolic function, Cell metabo. 23 (2016) 454–466.

[32]. Zhou WJ, Geng ZH, Chi S, Zhang W, Niu XF, Lan SJ, Ma L, Yang X, Wang LJ, Ding YQ, Geng JG, Slit-Robo signaling induces malignant transformation through Hakai-mediated E-cadherin degradation during colorectal epithelial cell carcinogenesis, Cell Res. 21 (2011) 609–626. [PubMed: 21283129]

[33]. Gu F, Ma Y, Zhang J, Qin F, Fu L, Function of Slit/Robo signaling in breast cancer, Front. Med 9 (2015) 431–436. [PubMed: 26542734]

[34]. Huang Z, Wen P, Kong R, Cheng H, Zhang B, Quan C, Bian Z, Chen M, Zhang Z, Chen X, Du X, Liu J, Zhu L, Fushimi K, Hua D, Wu JY, USP33 mediates Slit-Robo signaling in inhibiting colorectal cancer cell migration, Int. J. Cancer 136 (2015) 1792–1802. [PubMed: 25242263]

[35]. Li S, Huang L, Sun Y, Bai Y, Yang F, Yu W, Li F, Zhang Q, Wang B, Geng JG, Li X, Slit2 promotes angiogenic activity via the Robo1-VEGFR2-ERK1/2 pathway in both in vivo and in vitro studies, Invest. Ophthalmol. Vis. Sci 56 (2015) 5210–5217. [PubMed: 26244297]

[36]. Wu W, Wong K, Chen J, Jiang Z, Dupuis S, Wu JY, Rao Y, Directional guidance of neuronal migration in the olfactory system by the protein Slit, Nature 400 (1999) 331–336. [PubMed: 10432110]

[37]. Wang LJ, Zhao Y, Han B, Ma YG, Zhang J, Yang DM, Mao JW, Tang FT, Li WD, Yang Y, Wang R, Geng JG, Targeting Slit–roundabout signaling inhibits tumor angiogenesis in chemical-induced squamous cell carcinogenesis, Cancer Sci. 99 (2008) 510–517. [PubMed: 18201275]

[38]. Han HX, Geng JG, Over-expression of Slit2 induces vessel formation and changes blood vessel permeability in mouse brain, Acta Pharmacol. Sin 32 (2011)

[39]. Nieminen T, Toivanen PI, Laakkonen JP, Heikura T, Kaikkonen MU, Airenne KJ, Ylä-Herttuala S, Slit2 modifies VEGF-induced angiogenic responses in rabbit skeletal muscle via reduced eNOS activity, Cardiovasc. Res 107 (2015) 267–276. [PubMed: 26002231]

[40]. Han X, Zhang MC, Potential anti-angiogenic role of Slit2 in corneal neovascularization, Exp. Eye Res 90 (2010) 742–749. [PubMed: 20298689]

[41]. Bocca C, Novo E, Miglietta A, Parola M, Angiogenesis and fibrogenesis in chronic liver diseases, Cell Mol. Gastroenterol. Hepatol 1 (2015) 477–488. [PubMed: 28210697]

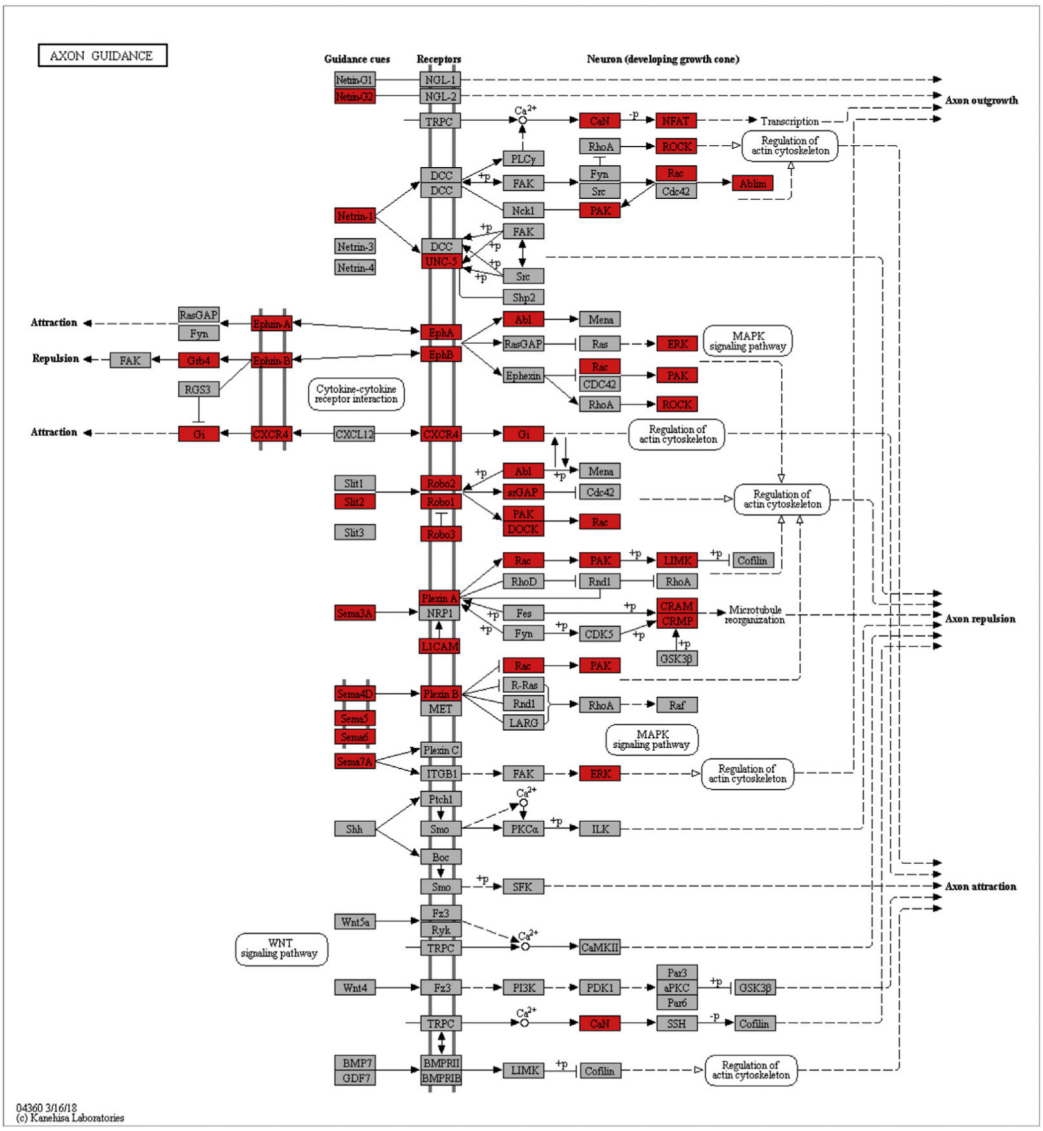

Fig. 1.

Transcriptomic analysis of axon guidance signaling pathways in liver fibrogenesis. Animal model of hepatic fibrosis was induced by diethylnitrosamine (DEN, i.p., 10 mg/kg/week) or thioacetamide (TAA, 100 mg/kg, i.p., three times per week) for 14 weeks. Liver samples collected from the control (N = 3) and the treatment groups (N = 5 per group) at 3, 6, 9, 14 weeks post DEN or TAA treatment for high throughput RNA sequencing. Pathway analysis of the differentially expressed genes that were sustainable up-regulated in fibrotic livers was performed based on latest Kyoto Encyclopedia of Genes and Genomes (KEGG) database. Differentially expressed genes belonging to the axon guidance signaling pathways that were up-regulated in both DEN and TAA models were mapped (red). The threshold of significance was defined as *P* value < 0.01 and FDR < 0.05. (For interpretation of the references to color in this figure legend, the reader is referred to the web version of this article.)

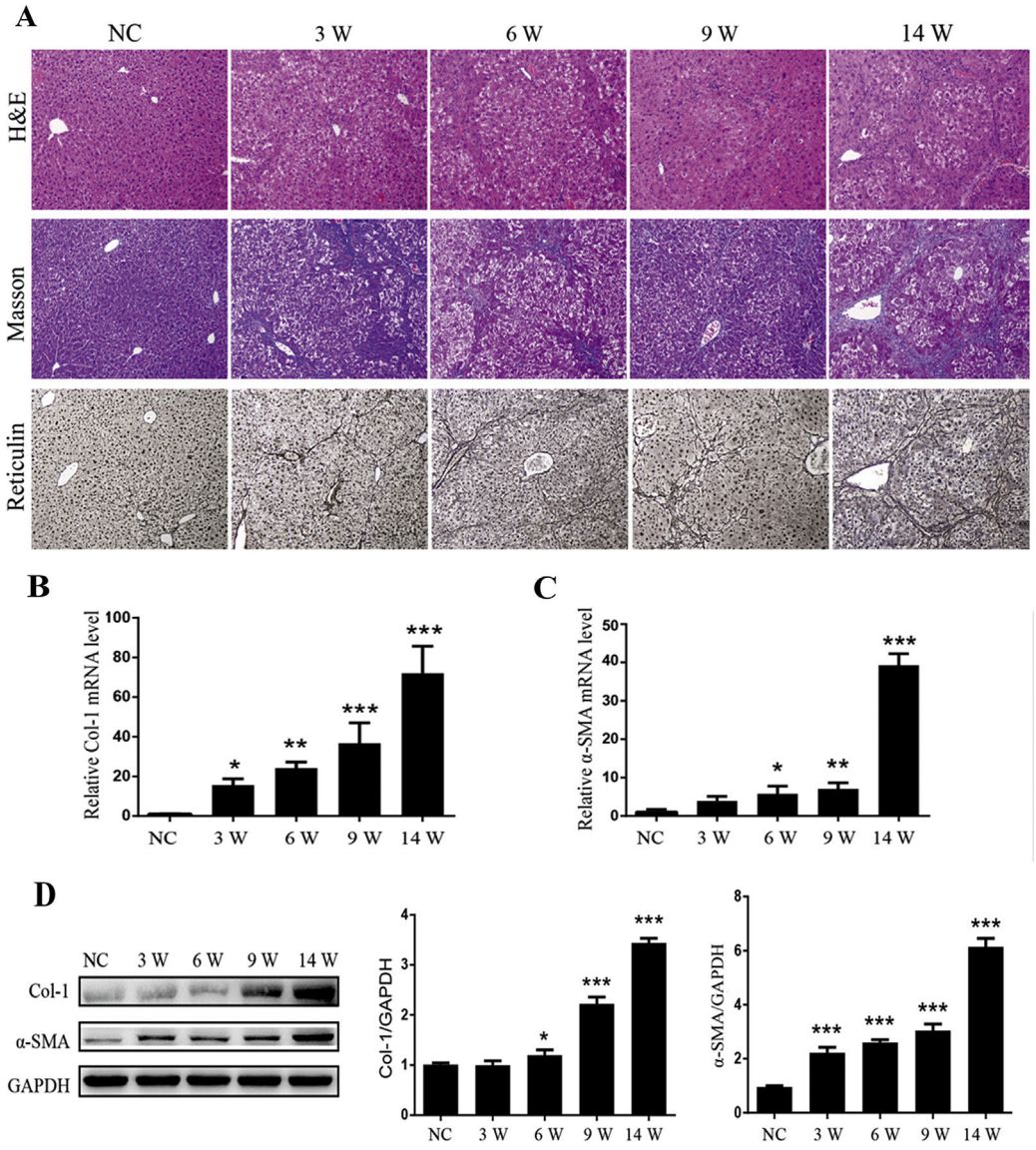

Fig. 2.

Induction of experimental liver fibrosis by thioacetamide (TAA) in mice. (A) Morphological examination for the progression of liver fibrosis on liver tissue sections from normal mice (N = 3) and mice with TAA treatment for 3, 6, 9, 14 weeks (N = 5 per group). Representative histological pictures of Hematoxylin and eosin (H& E) (upper panels), Masson's trichrome (middle panels) and Reticulin staining (lower panels) are shown. Magnification was 10×; (B) Determination of the mRNA levels of collagen 1 (Col-1) by real time quantitative PCR (RT-qPCR) in the livers of normal mice (N = 3) and mice with TAA treatment for 3, 6, 9, 14 weeks (N = 5 per group). (C) Determination of the mRNA levels of α-SMA in the livers of different groups by RT-qPCR; (D) Representative Western blot profile of Col-1 and α-SMA protein expression in the livers of different groups. Semi-quantitative analyzed Col-1 and α-SMA protein signals was standardized against the corresponding GAPDH signal. Values are presented as mean ± SD of N = 3 per group in three independent experiments. *$P < 0.05$,

** $P < 0.01$, and *** $P < 0.001$ compared to NC. NC: normal control mice; 3W, 6W, 9W, 14W: mice with TAA treatment for 3, 6, 9, 14 weeks, respectively.

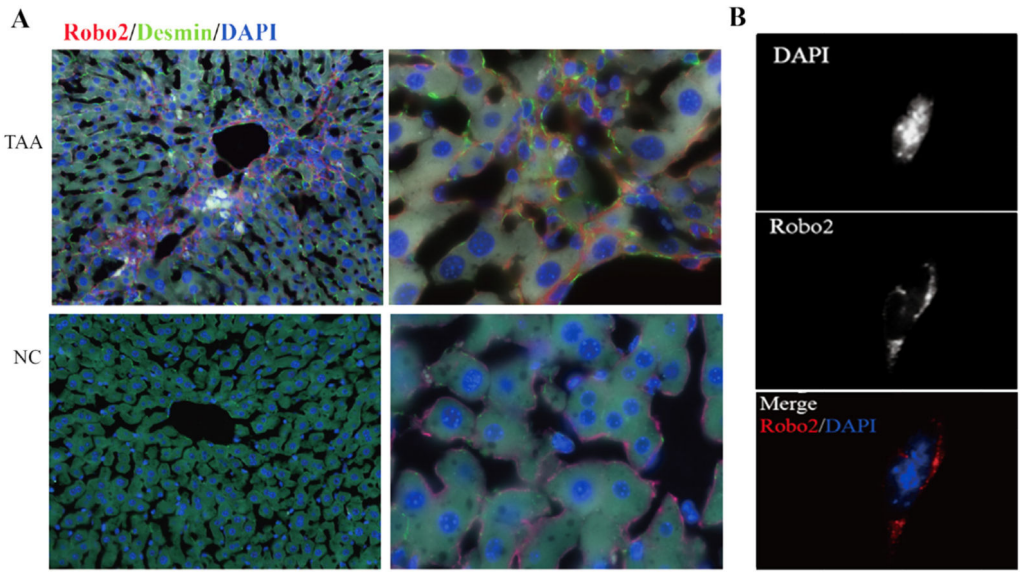

Fig. 3.

Immunofluorescence staining of Robo2 in normal and fibrotic liver tissues, and a mouse hepatic cell line JS1. (A) The expression and distribution of Robo2 correlated well with the fibrotic septa in fibrotic livers, and were on the surface of cells shown double-positive staining with desmin in cytoplasm. TAA (upper panels): fibrotic liver with TAA treatment for 6 weeks; NC (lower panels): normal liver. Left panels: 20 × magnification; right panels: 100 × magnification; (B) Localization of Robo2 on the cells surface of JS1. Magnification was 100×.

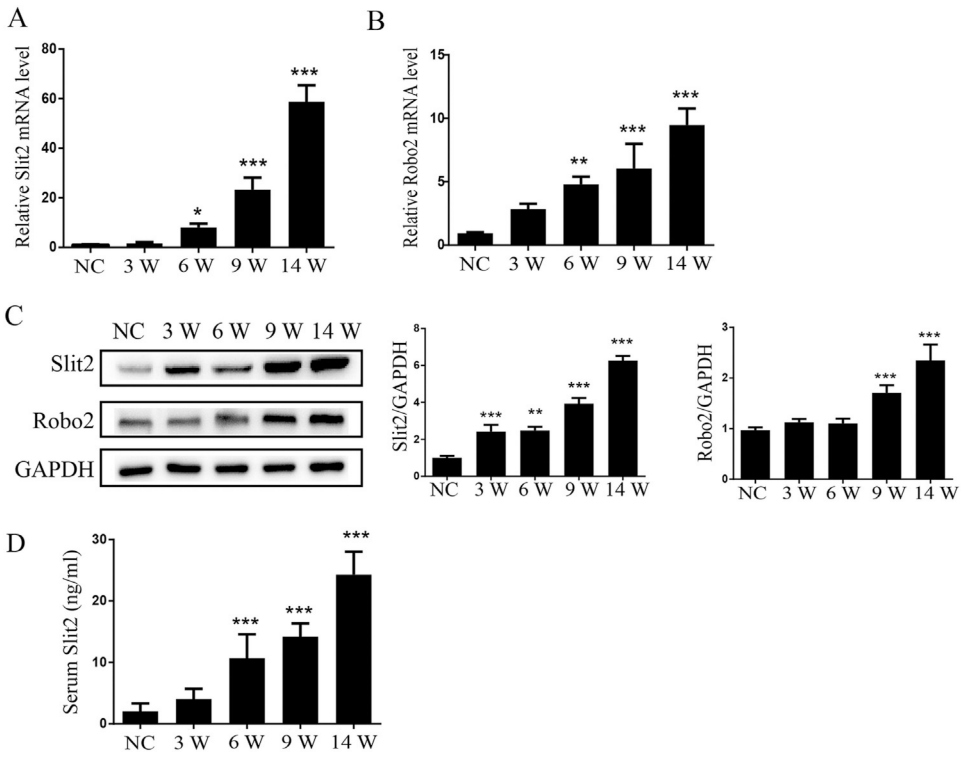

Fig. 4.

Upregulation of serum Slit2 level and liver Robo2 expression in mice with liver fibrosis. (A) Determination of mRNA levels of Slit2 in normal mice (N = 3) and mice with TAA treatment for 3, 6, 9, 14 weeks (N = 5 per group) by real time quantitative PCR (RTqPCR); (B) Determination of the mRNA levels of Robo2 in the livers of different groups by RT-qPCR; (C) Representative Western blot profile of Slit2 and Robo2 in the livers of different groups. The results are expressed as ratios of Col-1 or α-SMA to GAPDH semi-quantitative signals. (D) Evaluation of the serum levels of Slit2 in normal control mice (N = 3) and mice with TAA treatment for 3, 6, 9, 14 weeks (N = 5 per group) by enzyme-linked immunosorbent assay (ELISA). All samples were assayed triplicate repeats and values were expressed as mean ± SD. $*P < 0.05$, $**P < 0.01$, and $***P < 0.001$ compared to NC. NC: normal control mice; 3W, 6W, 9W, 14W: Mice with TAA treatment for 3, 6, 9, 14 weeks, respectively.

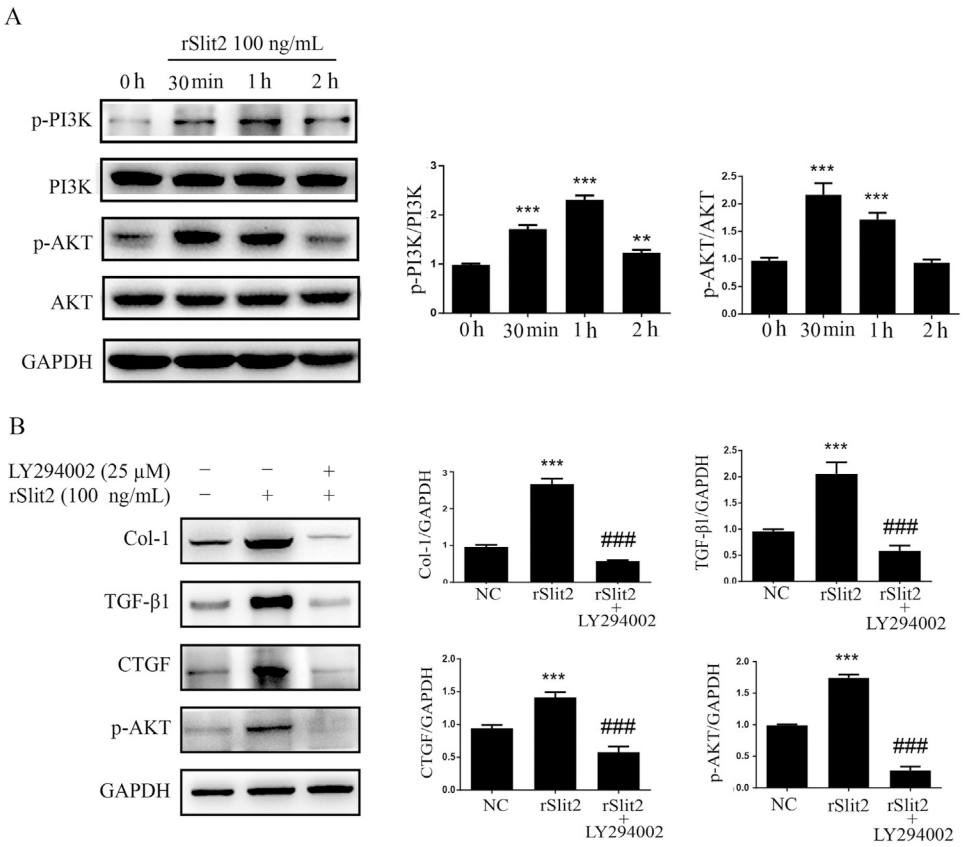

Fig. 5.

Induction of the fibrogenic factors expression in HSCs by recombinant Slit2 (rSlit2) via PI3K/Akt pathway. (A) Representative Western blot profile of phosphorylated or total PI3K and Akt in JS1 cells with rSlit2 (100 ng/mL) treatment for 0 h, 30 min, 1 h and 2 h are shown. Results are expressed as ratios of semiquantitative analyzed phosphorylated PI3K or Akt signals to their corresponding total proteins. rSlit2 treatment increases PI3K and Akt phosphorylation in JS1 cells. Data are presented as mean ± SD of N = 3 per group in three independent experiments. $^{**}P < 0.01$, and $^{***}P < 0.001$ compared to 0 h; (B) Representative Western blot profile for the effect of rSlit2 (100 ng/mL) on the protein expression of Col-1, TGF-β1 and CTGF in JS1 cells with or without LY294002 (25 μM) pretreatment. Results are expressed as ratios of Col-1, TGF-β1, CTGF and p-AKT signals to that of GAPDH. Data are presented as mean ± SD of N = 3 per group in three independent experiments. $^{***}P < 0.001$ compared to NC; $^{\#\#\#}P < 0.001$ compared to cells treated with rSlit2; NC: control cells treated with vehicle; rSlit2: cells treated with rSlit2 (100 ng/mL); rSlit2 + LY294002: cells treated with LY294002 (25 μM) and rSlit2 (100 ng/mL).

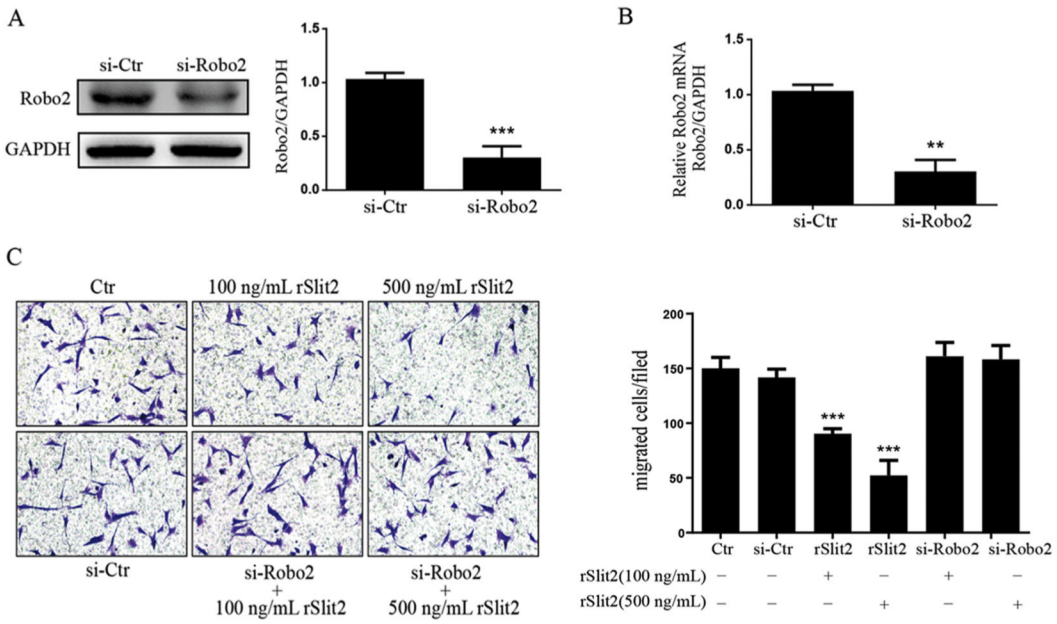

Fig. 6.

Slit2/Robo2 signaling inhibited HSCs migration. Transfection of Robo2 siRNA (si-Robo2) in JS1 cells efficiently decreased Robo2 protein and mRNA expression. (A) Representative Western blot profile of Robo2 protein level in Robo2 siRNA transfected JS1 cells is shown. Data are presented as the ratio of Semi-quantitative analyzed Robo2 signal to that of GAPDH. ***$P < 0.001$ compared to the control siRNA transfected cells (si-Ctr); (B) The mRNA expression of Robo2 were determined by real time quantitative PCR (RT-qPCR). The expression levels were normalized to GAPDH. Data are presented as mean ± SD of N = 3 per group in three independent experiments. **$P < 0.01$ compared to the control siRNA transfected cells (si-Ctr). (C) Representative pictures for the effect of rSlit2 (100 ng/mL and 500 ng/mL) with or without Robo2 siRNA knockdown (si-Robo2) on HSCs migration are shown. rSlit2 dose dependently inhibited JS1 cells migration. The inhibitory effect of rSlit2 on HSCs migration was abrogated by Robo2 siRNA knockdown. Magnification was 20×. Data are presented as mean ± SD of N = 3 per group in three independent experiments. ***$P < 0.001$ compared to si-Ctr.

Table 1

Pathways analysis of transcriptomic data associated with liver fibrosis progression in diethylnitrosamine (DEN) model.

Pathway ID	Pathway term	DifGene	*P*-value	FDR	Enrichment
PATH:04510	Focal adhesion	77	2.12173E-11	5.41040E-09	2.683956267
PATH:04060	Cytokine-cytokine receptor interaction	83	2.79329E-09	2.37430E-07	2.268450051
PATH:04151	PI3K-Akt signaling pathway	100	5.46857E-09	3.48622E-07	2.06151743
PATH:04512	ECM-receptor interaction	38	1.14008E-07	4.84534E-06	3.080694586
PATH:04380	Osteoclast differentiation	47	1.33927E-07	4.87876E-06	2.670233206
PATH:05205	Proteoglycans in cancer	68	2.33252E-07	6.65913E-06	2.170978532
PATH:05200	Pathways in cancer	89	2.35038E-07	6.65913E-06	1.951862247
PATH:04014	Ras signaling pathway	68	3.03188E-07	7.73129E-06	2.151934861
PATH:04810	Regulation of actin cytoskeleton	66	3.71753E-07	8.61792E-06	2.164593301
PATH:04360	Axon guidance	48	4.65484E-07	9.89154E-06	2.530743412
PATH:04670	Leukocyte transendothelial migration	44	5.67287E-07	1.11275E-05	2.602243313
PATH:04514	Cell adhesion molecules (CAMs)	52	7.02364E-07	1.27931E-05	2.359724354

Note: Axon guidance signaling are listed within the significantly upregulated signaling pathways (partial).

Table 2

Pathways analysis of transcriptomic data associated with liver fibrosis progression in thioacetamide (TAA) model.

Pathway ID	Pathway term	DifGene	*P*-value	FDR	Enrichment
PATH:04512	ECM-receptor interaction	29	5.47E-12	1.37E-09	4.28409091
PATH:04510	Focal adhesion	45	4.83E-11	6.06E-09	2.87642046
PATH:04151	PI3K-Akt signaling pathway	54	2.32E-07	1.16E-05	2.04545455
PATH:05205	Proteoglycans in cancer	39	6.50E-07	2.33E-05	2.29434835
PATH:04390	Hippo signaling pathway	27	2.62E-05	0.00065699	2.33102125
PATH:05200	Pathways in cancer	44	0.00011124	0.00232667	1.7781155
PATH:04514	Cell adhesion molecules (CAMs)	26	0.0001237	0.00238836	2.17409949
PATH:04360	Axon guidance	23	0.00014333	0.00256977	2.28205563
PATH:04010	MAPK signaling pathway	37	0.00025801	0.00380942	1.81524656
PATH:04350	TGF-beta signaling pathway	17	0.00028484	0.00397196	2.53958121
PATH:04810	Regulation of actin cytoskeleton	31	0.00046624	0.0061593	1.87345041
PATH:04310	Wnt signaling pathway	24	0.00068317	0.00784191	2.01956272

Note: Axon guidance signaling are listed within the significantly upregulated signaling pathways (partial).